

On the Impact of Solvation on a Au/TiO₂ Nanocatalyst in Contact with Water

Matteo Farnesi Camellone and Dominik Marx

Lehrstuhl für Theoretische Chemie, Ruhr-Universität Bochum, 44780 Bochum, Germany

(Dated: March 22, 2013)

Water, the ubiquitous solvent, is also prominent in forming liquid-solid interfaces with catalytically active surfaces, in particular with promoted oxides. We study the complex interface of a gold nanocatalyst, pinned by an F-center on titania support, and water. The *ab initio* simulations uncover the microscopic details of solvent-induced charge rearrangements at the metal particle. Water is found to stabilize charge states differently from the gas phase as a result of structure-specific charge transfer from/to the solvent, thus altering surface reactivity. The metal cluster is shown to feature both “cationic” and “anionic” solvation, depending on fluctuation and polarization effects in the liquid, which creates novel active sites. These observations open up an avenue toward “solvent engineering” in liquid-phase heterogeneous catalysis.

Highly dispersed gold nanoparticles supported on oxides have been shown to catalyze a number of important reactions, including low-temperature CO oxidation and the water gas shift reaction [1, 2]. Reducible oxides, in particular titania (TiO₂), are ideal catalytic supports [3]. The size of the gold particles substantially affects the catalytic activity, suggesting the key importance of metal/support interactions on a nanometer scale [4]. Reactions, and in particular CO oxidation, are believed to occur at specific active Au sites at the Au/TiO₂ interface [5–8]. Although much is known regarding Au/TiO₂ catalytic activity in the presence of a gas phase, the complexity increases steeply when solvent is included.

Liquid-solid interfaces as such are relevant to many industrial applications of great significance, such as (photo-)catalysis, solar cells, gas sensors, or biocompatible devices. In heterogeneous catalysis, it has been shown that the presence of water increases the observed rate of CO oxidation [9, 10]. The degree of rate enhancement depends on the type of support used. In particular for the case of Au/TiO₂ catalysts it has been shown that their activity at about 3000 ppm H₂O is so high that full conversion of CO is reached [10]. Thus, the Au/TiO₂ surface displays a pronounced catalytic activity toward the water-gas-shift (WGS) reaction. This fundamental reaction represents a key reaction to produce extra H₂ fuel from steam reforming, which is reversible and exothermic, according to the following reaction: $\text{CO} + \text{H}_2\text{O} \rightleftharpoons \text{CO}_2 + \text{H}_2$. The so-called carboxyl and redox mechanisms have been proposed for the WGS reaction on metal/oxide surfaces; in the former mechanism the CO species reacts with terminal hydroxyl groups, whereas in the latter CO reacts with an O atom from OH dissociation or from the oxide support. In both mechanism proposed the starting point is a H₂O molecule that is initially adsorbed on the metallic cluster with its oxygen atom being attached to a metal atom.

Moreover, even large (as opposed to nanoscale) gold particles, which are usually catalytically inert, show considerable oxidation activity at aqueous conditions [11,

12]. Because of its high dielectric constant, water may actively participate in chemical reactions for instance by stabilizing ionic species, thus speeding up reactions at liquid-solid interfaces, which opens up novel avenues to improve the performance of traditional heterogeneous catalysis at the gas-solid interface. Recently, it has been shown that the selective oxidation of alcohols in aqueous phase over (TiO₂, C)-supported Au catalysts is facilitated by high pH conditions [13]. This water-based approach to heterogeneous catalysis offers a sustainable, environmentally benign, and cheap alternative to traditional processes that rely on both toxic and expensive inorganic oxidants and organic solvents [14]. Despite these promising experimental findings, much remains unknown at the molecular level about the impact of water as a solvent on the reactivity of these modern catalyst systems.

Several *ab initio* molecular dynamics (AIMD) [15] studies have been recently reported focussing on the fundamentals of the water-titania interface. For a water film on TiO₂(110) it has been shown that at least two distinct layers form: molecules in the first layer are sluggish and bind strongly to fivefold coordinated Ti sites, whereas those in the second layer interact only weakly with the substrate and diffuse rapidly [16], thus yielding a highly anisotropic interface [17]. Moreover, water was not seen to dissociate at the coverages examined. Upon studying the thermodynamics of de/protonation of the rutile-water interface using free energy perturbation methods, a value of 0.6 eV was found for the dissociation free energy of bulk water on defect-free rutile [18]. These studies thus show that the ideal TiO₂ surface is rather inert with respect to solvation by water. However, little is known about the interaction between water and defective or metal-supporting TiO₂ interfaces, being relevant to catalysis and industrial applications.

Here, we present large-scale AIMD simulations aimed to investigate solvent effects at a gold nanocluster pinned by an F-center on TiO₂(110) being in contact with liquid water. The aqueous solution is found to induce pronounced charge transfer and localization at the

nanocatalyst-liquid interface and stabilizes structures different from the gas phase. The $\text{TiO}_2(110)$ surface has been modeled by four $\text{O-Ti}_2\text{O}_2\text{-O}$ tri-layer (4×2) super-cell slabs separated by more than 15 Å. The most common point defects on the $\text{TiO}_2(110)$ rutile surface are oxygen vacancies in the twofold coordinated O rows [3]. Therefore, a Au_{11} nanocluster was grown on $\text{TiO}_2(110)$ where an F-center created by a surface O vacancy acted as anchoring site for initial Au nucleation; note that this blocks the O defect to interact with water and thus prevents splitting of water molecules at this F-center. The lowest energy structure of Au_{11} adsorbed on a reduced rutile surface and employed in the present study is shown in Fig. 1(c)). In order to create the $\text{Au}_{11}/\text{TiO}_2$ -water interface, the space between the slabs has been fully filled with 53 H_2O molecules (see Fig. 1(a)). It has been shown that Au_7 is the smallest Au cluster on rutile $\text{TiO}_2(110)$ with a measurable reaction rate for CO combustion [19]. The Au_{11} model, although being a simplification of the nanometersized clusters on $\text{TiO}_2(110)$, appropriately mimics the active sites located at the nanogold/oxide interface where the oxidation process takes place [6, 20].

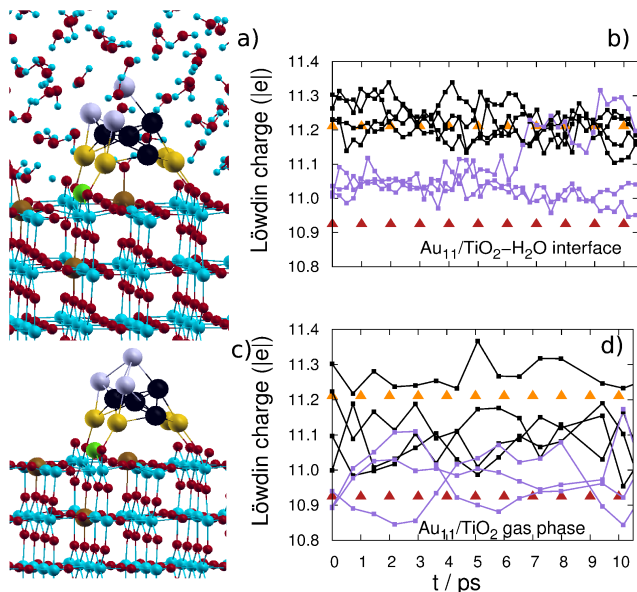


FIG. 1: Ball and stick model of the Au_{11} nanocluster pinned by an F-center on the $\text{TiO}_2(110)$ oxide surface in contact with liquid water (a) and with a gas phase (c). Red, big blue, small blue and brown spheres are O, Ti, H and Ti^{3+} sites, respectively, whereas the surface O vacancy is shown in green. Violet, black and yellow spheres correspond to top, middle and bottom Au sites of the Au_{11} nanocluster, respectively. Time evolution of the Löwdin charges of the top (violet lines) and middle (black lines) Au atoms of the supported gold nanocluster in liquid water (b) and in the gas phase (d). Red and orange triangles correspond to reference Löwdin charges computed for a single $\text{Au}^+(\text{aq})$ cation (10.924 $|e|$) and $\text{Au}^0(\text{aq})$ atom (11.210 $|e|$) in liquid water, respectively.

The binding of the Au_{11} cluster on the reduced $\text{TiO}_2(110)$ support entails a strong charge rearrangement at the metal/oxide contact (see Supporting Figure 1), the adsorption energy being -2.19 eV. In the case of an isolated O vacancy on the stoichiometric $\text{TiO}_2(110)$ surface, the charge neutrality is maintained by the presence of two Ti^{3+} ions thus creating an F-center. Spin density and bonding charge analyses reveal that the Au_{11} cluster, once adsorbed, leaves a reduced substrate with three Ti^{3+} ions, and $\sim 0.4 |e|$ are transferred from the metal cluster to the oxide. This results into a slightly positively charged $\text{Au}_{11}^{\delta+}$ cluster supported by a reduced $\text{TiO}_2(110)$ oxide surface.

In order to reveal the solvent-induced charge rearrangement at the metal-liquid contact, we have performed PBE + U AIMD simulations of the $\text{Au}_{11}/\text{TiO}_2(110)$ nanocatalyst in aqueous solution. Additionally, corresponding gas phase simulations have been carried out to provide the solvent-free reference situation. In both cases the finite temperature dynamics preserves three reduced Ti^{3+} sites (see Supporting Figure 2). Snapshots of the AIMD simulations have been collected every ~ 0.2 ps thus generating a set of representative configurations for electronic structure analyses. In the following, we will refer to Au atoms of the supported Au_{11} nanocluster as top, middle and bottom sites, which are depicted as violet, black and yellow spheres in Fig. 1, respectively. A detailed investigation of the interaction between H_2O molecules and the bare oxide surface far from the supported metal cluster is out of the focus of this study, but we note in passing that our AIMD simulations are in agreement with those of [16–18] in the regions. In particular, water at the liquid-oxide contact is slow, strongly bonded to fivefold coordinated Ti sites, and is not seen to dissociate.

The charge dynamics of the Au sites was extracted by computing, as a function of time, the Löwdin charges, see Fig. 1, where violet and black lines correspond to the charge evolution of top and middle Au atoms, respectively. As demonstrated by Fig. 1(b), two distinct charge patterns, corresponding to top and middle Au sites, can be clearly distinguished in aqueous solution; note that Au atoms in direct contact with TiO_2 (yellow spheres in Fig. 1(a)) cannot be solvated by the liquid phase and thus do not exhibit a clear trend. The average charges on top and middle Au atoms are 11.028 ± 0.006 and $11.220 \pm 0.006 |e|$, respectively (see Supporting Table 1 for statistical analysis). It is noted in passing that a very similar charge separation has been found for a gold cluster of different size and shape using an $\text{Au}_{13}/\text{TiO}_2(110)$ nanocatalyst in contact with water. Interestingly, at around 6 ps a considerable amount of charge is transferred to a specific top Au site due to solvent fluctuations, which reaches a value that is typical of middle Au atoms, see Fig. 1(b). In stark contrast, no such charge separation and fluctuation effects can be identified in the

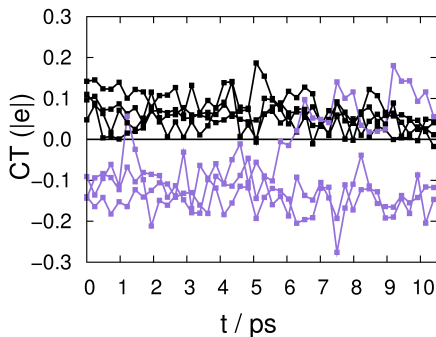


FIG. 2: **Dynamics of the water \rightleftharpoons nanocluster charge transfer (CT).** Violet and black lines correspond to top and middle Au atoms, respectively

gas phase reference dynamics in Fig. 1(d). We conclude that the liquid phase promotes and stabilizes a net charge separation in the supported Au cluster, where top and middle atoms can be clearly distinguished on the basis of their electronic structure. As a result, water steers the Au sites towards either one or the other preferred charge value, depending on their specific location within the nanocluster and going hand in hand with different solvation patterns, *vide infra*.

To further characterize this puzzling process we have quantified the amount of charge transfer (CT) from Au atoms to the aqueous solution and back using Bader analysis [23, 24]. For this purpose we have computed the difference between the Bader charges of the Au atoms in the fully solvated $\text{Au}_{11}/\text{TiO}_2(110)$ -water system and those of the corresponding $\text{Au}_{11}/\text{TiO}_2(110)$ gas phase system, where the latter is obtained upon removing the solvent while keeping all atomic positions fixed. As depicted in Fig. 2 we find that top Au sites transfer charge to the solvent, with an average CT of about $0.13 \pm 0.05 |e|$, while middle Au atoms attract about $0.06 \pm 0.03 |e|$ per Au atom from water.

In view of these pronounced CT effects, we probe solvent-induced morphology changes of the metal cluster with respect to the gas phase. A set of trajectory configurations of the solvated nanocatalyst has been selected where water has been removed before quenching and optimizing the remaining $\text{Au}_{11}/\text{TiO}_2(110)$ system. In order to generate the proper gas phase reference, $\text{Au}_{11}/\text{TiO}_2(110)$ in the absence of water has been run at the same temperature of 450 K before applying the same quenching protocol; note that this is the relevant experimental temperature used for selective liquid-phase alcohol oxidation in aqueous solution using gold/titania catalysts. In case of the quenched solvated interface, the same local minima and no significant change in the Löwdin charges were observed as in the solvated state. However, the gas phase reference system yielded several local minima with significant changes of both the real-

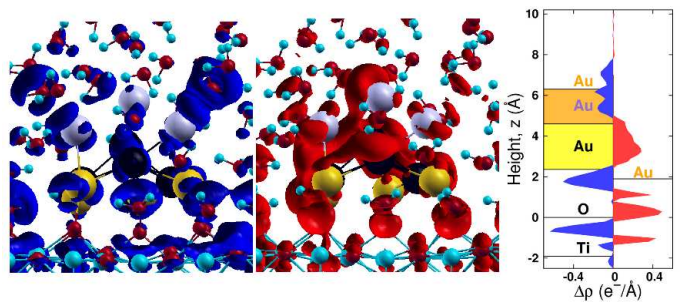


FIG. 3: **Water-induced charge flow.** Left and central panels: charge difference, $\Delta\rho(\vec{r})$, for a representative snapshot of the $\text{Au}_{11}/\text{TiO}_2(110)$ -water interface. Electron depletion/accumulation is depicted by blue/red isosurfaces at $\pm 0.02 |e|/\text{\AA}^3$. Right panel: charge difference integrated in planes perpendicular to the surface, $\Delta\rho(z)$, as a function of the height, z .

space structure and the Au charges (see Supporting Figures 3 and 4). These findings show that the liquid phase stabilizes structures and charge states within nanogold that are distinctly different from those observed in the gas phase, which eventually induces novel morphologies and active sites, respectively, due to solvation.

Let us now investigate the solvent-induced electronic charge redistribution at the nanocatalyst. In the following, we refer the electronic charge density of the solvated $\text{Au}_{11}/\text{TiO}_2(110)$ -water system to that of the isolated one, $\text{Au}_{11}/\text{TiO}_2(110)$, and the separated solvation water. We thus compute the difference, $\Delta\rho(\vec{r})$, between the charge densities of the combined system and the separated components while freezing all atomic positions. A representative example of water-induced charge flow is depicted in Fig 3, where the positive (negative) component of the charge difference $\Delta\rho_{+(-)}(\vec{r})$ is shown by red (blue) isosurfaces. This reveals that charge depletion (blue) occurs mainly on top Au atoms, whereas additional electron charge (red) prefers to accumulate on middle Au sites. Furthermore, charge depletion and accumulation visible at the oxide-water contact can be traced back to the interaction between water and the $\text{TiO}_2(110)$ oxide support. Here charge depletion occurs mainly on top of surface O atoms to which H_2O molecules point with their H atoms, whereas charge accumulates close to five-fold coordinated Ti atoms, being in turn coordinated by water O atoms. This is quantified by considering the charge redistribution perpendicular to the support, $\Delta\rho(z)$ (see Fig. 3). Here $\Delta\rho(z)$ is the sum of the positive and negative charge density components and integrated in planes perpendicular to the surface. This quantitative analysis reveals that, on the one hand, there is a net charge transfer of $\sim 0.22 |e|$ from top Au atoms to H_2O molecules (obtained by integrating $\Delta\rho(z)$ within the shaded orange area in Fig. 3), leading to slightly positively charged $\text{Au}^{\delta+}$ atoms at the corresponding sites.

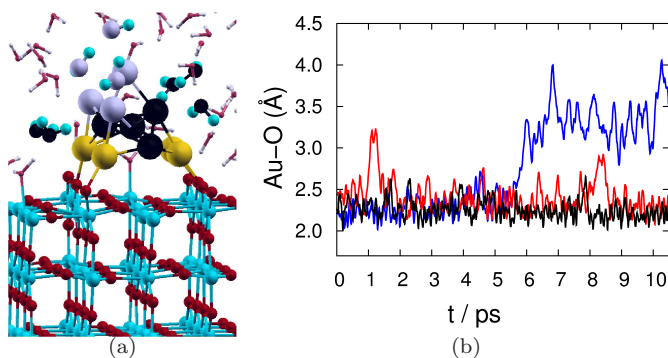


FIG. 4: **Snapshot of a typical hydration structure for the $\text{Au}_{11}/\text{TiO}_2(110)$ nanocatalyst in aqueous solution.** In the cationic/anionic solvation pattern H_2O molecules (violet/black spheres) are pointing with their O/H atoms toward top/middle Au atoms (violet/black spheres) (a). (b) Time evolution of the Au-O distances of the gold atoms depicted in violet.

On the other hand, there is a reverse charge flow of $\sim 0.37 |e|$ from water to middle Au atoms (see yellow area in Fig. 3), thus creating partially negatively charged $\text{Au}^{\delta-}$ atoms upon solvation. Similar results were obtained for all the representative structures sampled along the trajectory. This can be compared to the average negative and positive CT obtained from the Bader analysis. In total, this amounts to a structure-specific charge exchange between metal and water of -0.34 and $+0.46 |e|$, in qualitative agreement with the charge difference analysis. As a result, top and middle Au sites experience opposite charge flow upon interaction with the solvent, as clearly shown in Fig. 3, which connects to a peculiar solvation pattern.

We thus conclude by discussing the solvation pattern around the $\text{Au}_{11}/\text{TiO}_2(110)$ nanocatalyst, see Fig. 4(a), which is found to feature both so-called “cationic” and “anionic” solvation depending on fluctuation and polarization effects. This is similar to what we have observed previously for a single $\text{Au}^+(\text{aq})$ cation and neutral atom, $\text{Au}^0(\text{aq})$, in aqueous bulk solution [25]. In particular, the Au^+ aqua ion forms a quasi-linear molecular structure, $\text{H}_2\text{O}-\text{Au}^+-\text{OH}_2$, in which two water molecules are firmly bound through their oxygens to the Au^+ site, as expected for a cation, yielding an Au^+-O distance of ~ 2.04 Å. Upon adding an electron to Au^+ to yield Au^0 , we found that its solvation pattern changes distinctly. The latter features two distinct regions, supporting a Janus-type behavior. In one region a typical anionic solvation pattern prevails where two water molecules are pointing with their H atoms toward the metal. In other regions water binds via its O site to the $\text{Au}^0(\text{aq})$, thus giving rise to a typical cationic solvation pattern.

Around the nanocatalyst, two distinct solvation patterns corresponding to different Au charge states can be identified. The solvation around middle Au atoms con-

sists of H_2O molecules pointing with their H atoms toward the Au atoms like in an anionic solvation shell. In addition, several water exchange processes are observed as for $\text{Au}^0(\text{aq})$ in the bulk [25]. At variance with those sites, the solvation around top Au atoms features a typical cationic solvation pattern, where a single H_2O molecule points to a top Au atom *via* its O site. A projected density of states analysis reveals that the interaction results from the overlap between the $\text{Au}(d)$ and $\text{O}(p)$ states of the respective gold and oxygen sites. Interestingly, no H_2O exchange processes are observed in this case again in line with the $\text{Au}^+(\text{aq})$ cation case [25]. As depicted in Fig. 1, the average Löwdin charges of top and middle Au sites are in qualitative agreement to those computed for a single gold cation ($10.924 |e|$) and neutral gold atom ($11.210 |e|$) in aqueous bulk solution. Based on this comparison, we are in a position to explain the sudden switch of the Löwdin charge involving a specific top Au atom and taking place at ~ 6 ps in Figs. 1(b) and 2. In Fig. 4(b) we plot the distances between the top Au atoms with typical “cationic” solvation pattern and the O atom of its solvating H_2O molecule. This demonstrates that two Au atoms are always “bonded” to the same H_2O molecule along the full trajectory, the time-averaged distances between Au and O sites being 2.25 and 2.35 Å. The situation is very different at the third top Au site. This Au atom is initially cationically solvated yielding a Au-O distance around 2.3 Å. At ~ 6 ps the H_2O molecule rearranges and points to the same gold atom with one of its H atoms, a fluctuation which induces the change of charge state of this Au site discussed earlier. This reveals the intimate connection between the creation of excess charge at specific nanocluster sites and the preferential orientation of the interfacial water molecules. As discussed in the introduction for the carboxyl and redox mechanisms proposed for the WGS reaction on metal/oxide surfaces, the first step involves H_2O molecules that are initially adsorbed on the metal cluster such that their O atoms are coordinated to an Au site. Therefore our simulations suggest that top site Au atoms, which feature a typical “cationic” solvation pattern at the water-gold interface, are the most promising candidates for being the active site for CO oxidation via the WGS reaction, whereas “anionically” coordinated Au sites are expected to be chemically inert. The very same argument will hold for other liquid-phase catalytic reactions – thus providing a novel mechanism to create active sites at catalyst–water interfaces in much more general terms.

In conclusion, finite temperature PBE + U simulations have been employed to investigate solvent-metal interactions on the gold/titania nanocatalyst in liquid water. Comparing our liquid phase to gas phase and bulk solvation reference data demonstrates that interfacial water alters both the structure and electronic properties of the

supported metal cluster in a significant way, including the creation of active sites. The fundamental phenomena observed will have a profound impact on understanding the role of solvent in heterogeneously catalyzed liquid-phase reactions, where de- and re-solvation processes play a key role.

Methods

All calculations have been performed using spin-polarized PBE + U [26], and ultrasoft pseudopotentials [27] as implemented in CPMD [28] and Quantum Espresso [29]. In line with our previous work [21, 22, 30], the value of $U = 4.2$ eV was adopted. We have carefully checked the charge distribution dependence on U by re-computing the Löwdin charges of the top and middle Au atoms of the supported gold nanocluster in liquid water for selected snapshots along the trajectory shown in Fig. 1(b) using four different U values and found no significant change (see Supporting Material for data).

The AIMD simulations [15] used Car–Parrinello propagation, the canonical ensemble was established at 450 K with a Nosé–Hoover chain thermostat, and about ~ 10 ps trajectories have been generated for analysis (see Supporting Material for details).

Corresponding Author

E-mail: matteo.farnesi@theochem.rub.de

Acknowledgements

We thank Martin Muhler for fruitful discussions. Partial financial support from Research Department “Interfacial Systems Chemistry” and the Cluster of Excellence RESOLV (EXC 1069) funded by Deutsche Forschungsgemeinschaft is gratefully acknowledged. Computational resources were provided by NIC (Jülich), BOVILAB@RUB (Bochum), RV–NRW as well as PRACE (FERMI at Cineca).

Supporting Information

Detailed descriptions of methods used for the calculations, model system and much additional analyses. This material is available free of charge via the Internet at <http://pubs.acs.org>.

- [1] Haruta, M.; Yamada, N.; Kobayashi, T.; Iijima, S. Gold Catalysts Prepared by Coprecipitation for Low-Temperature Oxidation of Hydrogen and of Carbon Monoxide. *J. Catal.* **1989**, *115*, 301-309.
- [2] Boccuzzi, F.; Chiorino, A.; Manzoli, M.; Andreeva, D.; Tabakova, T. FTIR Study of the Low-Temperature Water-Gas Shift Reaction on Au/Fe₂O₃ and Au/TiO₂ Catalysts. *J. Catal.* **1999**, *188*, 176-185.
- [3] Diebold, U. The Surface Science of Titanium Dioxide. *Surf. Sci. Rep.* **2003**, *48*, 53-229.
- [4] Valden, M.; Lai, X.; Goodman, D. W. Onset of Catalytic Activity of Gold Clusters on Titania with the Appearance of Nonmetallic Properties. *Science* **1998**, *281*, 1647-1650.
- [5] Liu, Z.-P.; Gong, X.-P.; Kohanoff, J.; Sanchez, C.; Hu, P. Catalytic Role of Metal Oxides in Gold-Based Catalysts: a First Principles Study of CO Oxidation on TiO₂ Supported Au. *Phys. Rev. Lett.* **2003**, *91*, 266102-266105.
- [6] Wang, J. G.; Hammer, B. Role of Au⁺ in Supporting and Activating Au₇ on TiO₂(110). *Phys. Rev. Lett.* **2006**, *97*, 136107-136110.
- [7] Green, I. X.; Tang, W.; Neurock, M.; Yates Jr. J. T. Spectroscopic Observation of Dual Catalytic Sites During Oxidation of CO on a Au/TiO₂ Catalyst. *Science* **2011**, *333*, 736-739.
- [8] Widmann, D.; Behm, R. J. Active Oxygen on a Au/TiO₂ Catalyst: Formation, Stability, and CO Oxidation Activity. *Angew. Chem. Int. Ed.* **2011**, *50*, 10241-10245.
- [9] Ojifinni, R. A.; Gong, J.; Froemming, N. S.; Flaherty, D.; Pan, M.; Henkelman, G.; Mullins, C. B. Carbonate Formation and Decomposition on Atomic Oxygen Pre-covered Au(111). *J. Am. Chem. Soc.* **2008**, *130*, 11250-11251.
- [10] Daté, M.; Okumura, M.; Tsubota, S.; Haruta, M. Vital Role of Moisture in the Catalytic Activity of Supported Gold Nanoparticles. *Angew. Chem. Int. Ed.* **2004**, *43*, 2129-2132.
- [11] Sanchez-Castillo, M. A.; Couto, C.; Kim, W. B.; Dumesic, J. A. Gold-Nanotube Membranes for the Oxidation of CO at Gas/Water Interfaces. *Angew. Chem. Int. Ed.* **2004**, *43*, 1140-1142.
- [12] Shang, C.; Liu, Z.-P. Origin and Activity of Gold Nanoparticles as Aerobic Oxidation Catalysts in Aqueous Solution. *J. Am. Chem. Soc.* **2011**, *133*, 9938-9947.
- [13] Zope, B. N.; Hibbitts, D. D.; Neurock, M.; Davis, R. J. Reactivity of the Gold / Water Interface During Selective Oxidation Catalysis. *Science* **2010**, *330*, 74-78.
- [14] Corma, A.; Garcia, H. Supported Gold Nanoparticles as Catalysts for Organic Reactions. *Chem. Soc. Rev.* **2008**, *37*, 2096-2126.
- [15] D. Marx and J. Hutter, *Ab Initio Molecular Dynamics: Basic Theory and Advanced Methods*, (Cambridge University Press, Cambridge 2009).
- [16] Liu, L.-M.; Zhang, C.; Thornton, G.; Michaelides, A. Structure and Dynamics of Liquid Water on Rutile TiO₂(110). *Phys. Rev. B* **2010**, *82*, 161415-161418(R).
- [17] Kimmel, G. A.; Baer, M.; Petrik, N. G.; VandeVondele, J.; Rousseau, R.; Mundy, C. J. Polarization - and Azimuth - Resolved Infrared Spectroscopy of Water on TiO₂(110): Anisotropy and the Hydrogen-Bonding Network. *J. Phys. Chem. Lett.* **2012**, *3*, 778-784.
- [18] Cheng, J.; Sprik, M. Acidity of the Aqueous Rutile TiO₂(110) Surface from Density Functional Theory Based Molecular Dynamics. *J. Chem. Theory Comput.* **2010**, *6*, 880-889.
- [19] Lee, S.; Fan, C.; Wu, T.; Anderson, S. L. CO Oxidation on Au_n/TiO₂ Catalysts Produced by Size-Selected Cluster Deposition. *J. Am. Chem. Soc.* **2004**, *126*, 5682-5683.
- [20] Kim, H. Y.; Lee, M.; Henkelman, G. CO Oxidation Mechanism on CeO₂ Supported Au Nanoparticles. *J. Am. Chem. Soc.* **2012**, *134*, 1560-1570.
- [21] Kowalski, P. M.; Farnesi Camellone, M.; Nair, N. N.; Meyer, B.; Marx, D. Charge Localization Dynamics Induced by Oxygen Vacancies on the TiO₂(110) surface. *Phys. Rev. Lett.* **2010**, *105*, 146405-146408.
- [22] Farnesi Camellone, M.; Kowalski, P. M.; Marx, D. Ideal, Defective, and Gold-Promoted Rutile TiO₂(110) Surfaces Interacting with CO, H₂, and H₂O: Structures, Energies, Thermodynamics, and Dynamics from PBE+U. *Phys. Rev. B* **2011**, *84*, 035413-035430.
- [23] R. F. W. Bader, *Atoms in Molecules A Quantum Theory*, (Oxford University Press, Oxford, 1990).
- [24] Henkelman, G.; Arnaldsson, A.; Jónsson, H. A Fast and Robust Algorithm for Bader Decomposition of Charge Density. *Comput. Mater. Sci.* **2006**, *36*, 354-360.

- [25] Farnesi Camellone, M.; Marx, D. Solvation of Au^+ Versus Au^0 in Aqueous Solution: Electronic Structure Governs Solvation Shell Patterns. *Phys. Chem. Chem. Phys.* **2012**, *14*, 937-944.
- [26] Perdew, J. P.; Burke, K.; Ernzerhof, M. Generalized Gradient Approximation Made Simple. *Phys. Rev. Lett.* **1996**, *77*, 3865-3868; *78*, 1396-1396(E).
- [27] Vanderbilt, D. Soft Self-Consistent Pseudopotentials in a Generalized Eigenvalue Formalism. *Phys. Rev. B* **1990**, *41*, 7892-7895.
- [28] J. Hutter *et al.*, CPMD, www.cpmid.org.
- [29] Giannozzi, P. *et al.*, QUANTUM ESPRESSO: a Modular and Open-Source Software Project for Quantum Simulations of Materials. *J. Phys.: Condens. Matter* **2009**, *21*, 395502; **Quantum Espresso**, www.pwscf.org.
- [30] Kowalski, P. M.; Meyer, B.; Marx, D. Composition, Structure, and Stability of the Rutile $\text{TiO}_2(110)$ Surface: Oxygen Depletion, Hydroxylation, Hydrogen Migration, and Water Adsorption. *Phys. Rev. B* **2009**, *79*, 115410-115425.